5.1 Scalar similarity functions: the influence of surface heterogeneity and entrainment

Arnold F. Moene*, Dirk Schüttemeyer and Oscar K. Hartogensis
Meteorology and Air Quality Group, Wageningen University

1. Introduction

In the study of turbulent flows in the atmospheric boundary layer dimensional analysis is widely used. The rationale behind this use is that dimensional analysis often gives simpler relationships between properties of the flow than would be given by the solution of the governing equations (for mean quantities, variances, fluxes etc.). For flows in the lower part of the atmospheric boundary layer the cornerstone of (the analysis of) experiments and modeling is Monin-Obukhov Similarity Theory (MOST).

For MOST the list of relevant variables is rather limited, which is both its strength and its weakness. To describe a statistic of a given quantity x (temperature, windspeed, etc.) the only relevant variables are the surface flux of that quantity $\overline{w'x'}$, the height above the ground z, the surface friction τ and the buoyancy parameter $\overline{w'\theta_v'}\frac{g}{T}$. Quantities that might be relevant as well are eliminated by a number of conditions:

- The flow should be stationary (i.e. $\frac{\partial x}{\partial t}$ is not relevant);
- The flow (or the surface) is horizontally homogeneous (i.e. horizontal derivatives of either x or $\overline{w'x'}$ are irrelevant);
- One should restrict the analysis to the region close to the ground: only the height z is relevant, not the distance to the top of the boundary layer; or alternatively: only the surface flux of the quantity under consideration is relevant, not the entrainment flux.

Unfortunately, reality is not as ideal as the assumptions mentioned above require. Therefore MOST is often applied in situations where one or more of the conditions are violated. The condition of stationarity is easily violated if one applies MOST during the period of sunrise and sunset. Horizontally homogeneous surfaces hardly exist, but it is often not clear whether the surface properties are so heterogeneous that this poses a problem for the application of MOST. Andreas et al. (1998) show that vegetation heterogeneities with a spatial scale of the order of a meter, influence the variance MOST relationships for humidity. de Bruin et al. (1993) report measurements in a semi-arid region. They suggest that, given the small surface flux for water vapour, the entrainment flux might become relevant, even at the surface.

One thing that both effects appear to have in common is that the similarity of temperature statistics is affected much less than the statistics of humidity. For the effect of entrainment this is not unlikely, since the entrainment ratio for temperature (or more precisely, potential virtual temperature) is bound within a narrow range: even if the entrainment flux of temperature would have an influence at the surface, that influence will scale well with the surface flux. On the other hand, one would expect that horizontal heterogeneity of evapotranspiration would be visible (through the Bowen ratio) in heterogeneity in the sensible heat flux as well. Andreas et al. (1998) however, state that the surface heat sources are -for their dataset- more homogeneously distributed than the sources of moisture. They attribute this -in part- to the homogeneity of the radiative forcing.

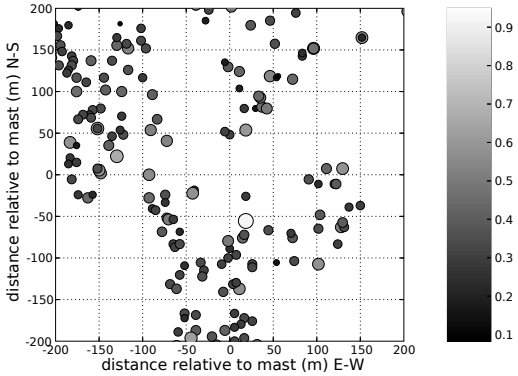

FIG. 1: Impression of distribution of trees in the savanah around the eddy-covariance mast in Ghana. The gray scales indicate the stem diameter in meter.

When one finds that certain scalar statistics do not obey MOST, this may be due to a violation of one or more of the conditions mentioned above. If it is obvious that both the condition of homogeneity *and* the condition regarding the absence of entrainment effects are violated, it remains to be seen which of those effects causes the deviations of the scalar statistics from MOST.

In this study we use two datasets of eddy-covariance data. One is gathered in Ghana (West-Africa) over a savannah landscape during the drying phase of the season (Schüttemeyer et al., 2006). Within one month the evapotranspiration decreases dramatically: at the start grass, bushes and trees transpire nearly unrestricted, whereas toward the end the grass has died, and only the trees are able to transpire without restrictions (figure 1 gives an impression of the tree density around the eddy-covariance mast). This data set comprises -possibly- two violations of the conditions for MOST:

*Corresponding author address: Arnold F. Moene, Meteorology and Air Quality Group, Wageningen University, Duivendaal 2, 6701 AP Wageningen; e-mail: arnold.moene@wur.nl

- The distribution of moisture sources becomes increasingly heterogeneous during the observation period

- The surface fluxes of water vapour and CO_2 decrease significantly, to the extent that the entrainment flux may become a relevant parameter in the surface layer as well.

The other data set was gathered during the CASES-99 experiment over relatively flat and homogeneous terrain in Kansas (Hartogensis et al., 2002). One property both the CASES dataset has in common with the data from Ghana is that the Bowen ratio increases considerably within a period of one month. Thus, although the first violation of MOST will not play a role in the CASES data, the second violation might.

The objective of this paper is to first determine to what extent statistics of temperature, humidity and CO_2 obey MOST, and whether this changes during the observation period. Secondly, we will identify whether deviations from MOST are attributable to surface heterogeneity or to entrainment effects.

The paper is organized as follows. In section 2 MOST is shortly reviewed and methods are presented that can be used to identify whether deviations from MOST are attributable to surface heterogeneity or to entrainment effects. In section 3 the data set is discussed as well as some details regarding the data analysis techniques. In section 4 the changes in surface fluxes and similarity functions during the observation period are presented. Furthermore, the causes for non-MOST behaviour are identified using the methods presented in section 2. Section 5 summarizes the conclusions of this study.

2. Theory

. In this section we will first present the similarity relationships for scalar fluctuations that are the subject of this paper. Then, the causes for the correlation coefficient between scalars to deviate from one will be investigated. Those deviations can be seen as an indicator of violations of the assumptions underlying MOST. Finally, we will present a number of quantities, derived from surface layer scalar measurements, that can be used to decide which violation of the assumptions of MOST is occurring.

2.1 *Monin-Obukhov Similarity Theory*

As stated in the introduction, MOST assumes that to describe a statistic of a given conserved quantity x (temperature, windspeed, etc.) the only relevant variables are the surface flux of that quantity $\overline{w'x'}$, the height above the ground z, the surface friction τ and the buoyancy parameter $\overline{w'\theta_v'}\frac{g}{T}$. The leads to the follow expression for the standard deviation of a scalar (σ_x):

$$\frac{\sigma_x}{|x_*|} = f_x\left(\frac{z-d}{L}\right) , \tag{1}$$

where

$$x_* \equiv \frac{\overline{w'x'}}{u_*} , u_* \equiv \sqrt{\frac{\tau}{\rho}} , L \equiv \frac{Tu_*^2}{kg\theta_{v*}} ,$$

d is the displacement height and ρ is the density of the air, T is the air temperature, g is the gravitational acceleration and k is the Von Karman constant. On the basis of dimensional analysis the limits for large (negative or positive) $\frac{z-d}{L}$ and small $\frac{z-d}{L}$ can be derived. For large negative values (free convection), the friction at the surface is no longer a relevant quantity, which leads to the prediction that

$$\frac{\sigma_x}{|x_*|} = A_{xu}\left(\frac{z-d}{L}\right)^{-1/3} \text{ for } \frac{z-d}{L} \ll -1 \tag{2}$$

For strongly stable conditions, the vertical motion is suppressed to that extent that the turbulence is not longer dependent on the distance to the wall. This eliminates z as a relevant parameter, predicting:

$$\frac{\sigma_x}{|x_*|} = A_{xs} \text{ for } \frac{z-d}{L} \gg 1. \tag{3}$$

Finally, for near-neutral conditions the buoyancy flux becomes irrelevant, which leads to

$$\frac{\sigma_x}{|x_*|} = A_{xn} \text{ for } \left|\frac{z-d}{L}\right| \ll 1. \tag{4}$$

Based on the asymptotic behaviour presented above, the following interpolation formulae are used for σ_x :

$$\frac{\sigma_x}{|x_*|} = c_{xu1}\left(1 - c_{xu2}\frac{z-d}{L}\right)^{-1/3} , \text{for } \frac{z-d}{L} < 0 \tag{5}$$

$$\frac{\sigma_x}{|x_*|} = c_{xs} , \text{for } \frac{z-d}{L} > 0 \tag{6}$$

2.2 *Origins of decorrelation of temperature with scalar*

One general observation regarding the validity of MOST is that the absolute value of the correlation coefficient between different conservative scalars should be very close to one for MOST to be valid (Hill, 1989). The rationale behind this is that the scalar should be transported by the same motions, and if the conditions of MOST are obeyed, there is no mechanism that could decorrelate the two scalars. Conversely, if the correlation coefficient differs from one, it can be assumed that one or more of the conditions for MOST are violated. Most cited violations are surface heterogeneity and the influence of entrainment in the surface layer (Roth and Oke, 1995; Katul et al., 1995; Andreas et al., 1998; Beljaars et al., 1983; de Bruin et al., 1993; de Bruin et al., 1991). Figure 2 illustrates those two mechanisms. In figure 2a, vegetated and non-vegetated patches are mixed. The vegetated patches are relatively wet (in terms of q-fluctuations) and cool, whereas the bare soil patches are dry and hot. This implies that in rising eddies, temperature and humidity will be anti-correlated. If we assume that the sinking eddies originate from a level where the horizontal inhomogeneities have vanished (i.e. above the blending height),

temperature and humidity will be positively correlated for downward motion. In figure 2b the effect of a difference in the entrainment regimes of temperature and humidity is depicted. The entrainment ratio for temperature (ratio of entrainment flux to surface flux, denoted by R_θ) is fixed within a limited range (approximately [-0.4,-0.2]). For that entrainment regime, the mean potential temperature appears to be a well-mixed quantity, giving a nearly constant value with height. Other scalars, however, may have completely different entrainment ratios (Druilhet et al., 1983; Sorbjan, 1991; Michels and Jochum, 1995; de Arellano et al., 2004). For entrainment ratios considerably larger than say 0.2 (in absolute value), the concentration of the scalar under consideration will not be well-mixed in the mixed-layer (see figure 3a, derived from LES results of Moeng and Wyngaard (1989)). This is due to the fact that the amount the scalar entering or leaving the boundary layer is so large, that the convection is not efficient enough to spread this local increase (or decrease) over the depth of the entire boundary layer. A consequence is that if large downdrafts enter the surface layer from within the mixed later (say from $z/z_i > 0.1$), they will cause a temperature fluctuation that is independent of the height from which the downdraft originates (because of constant θ with height). On the other hand, the magnitude of the fluctuation of a scalar with a large entrainment ratio *will* depend on the origin of the downdraft. Thus, under convective conditions, a dissimilarity in entrainment regime of temperature and humidity will cause a decorrelation of θ and q.

From the LES results of Moeng and Wyngaard (1989), the dependence of the correlation coefficient between two scalars in the surface layer (i.e. at $\frac{z}{z_i} = 0.01$ can be estimated. Figure 3b shows $r_{\theta q}$ for a number of realistic entrainment ratios for temperature. $r_{\theta q}$ is only close to one if the entrainment ratio for moisture is close to that of temperature. For a boundary layer drying by entrainment (see Mahrt (1991)), $r_{\theta q}$ can drop to 0.6. Whereas for moisture the entrainment ratio will usually be positive (positive surface flux and dry air aloft), for other scalars negative entrainment ratios may occur as well. In that case the decrease of $r_{\theta x}$ with R_x is even more pronounced.

2.3 *Consequences of decorrelation of temperature with scalar*

Katul and Hsieh (1999) show that in the case that $r_{\theta q} < 0$, and when humidity is treated as a passive scalar, the dimensionless moisture variance will always be larger than the dimensionless temperature variance. This asymmetry (i.e. that $\frac{\sigma_\theta}{\theta_*} \not> \frac{\sigma_q}{q_*}$) is due to that fact temperature is an active scalar and humidity a passive scalar. Only under extreme conditions the buoyancy effect of humidity would become relevant. Quantitatively, Katul and Hsieh (1999) predict that $\frac{\sigma_\theta}{\theta_*} = \frac{1}{r_{\theta q}} \frac{\sigma_q}{q_*}$. On the other hand, Lamaud and Irvine (2006) show that the asymmetry could also be reversed, for Bowen ratio's below 0.1. In that case $\frac{\sigma_\theta}{\theta_*} = r_{\theta q} \frac{\sigma_q}{q_*}$. The result of Lamaud and Irvine (2006) is

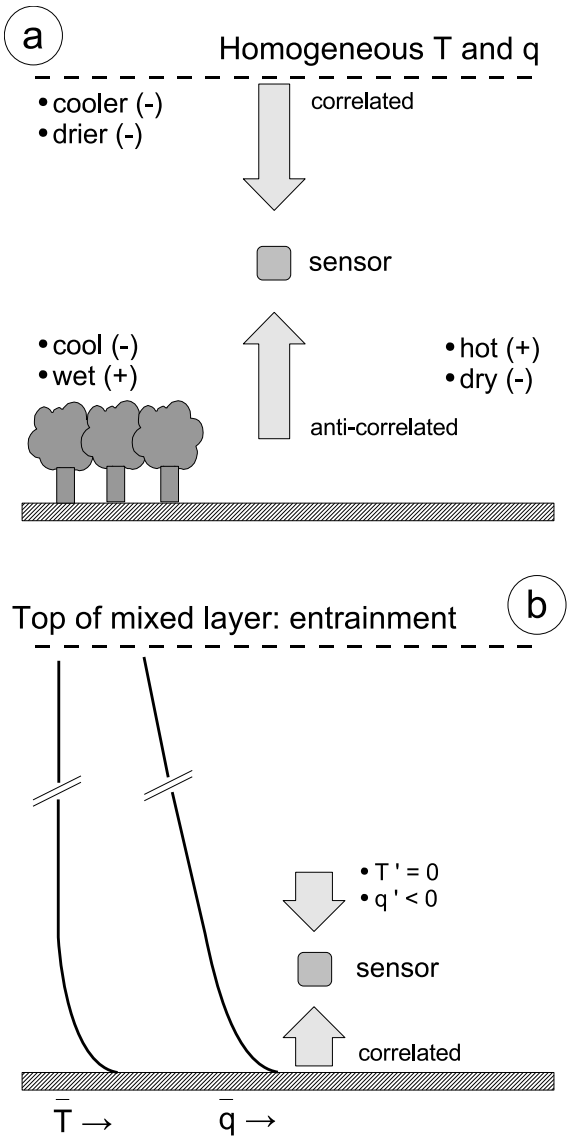

FIG. 2: Causes for decorrelation of temperature and humidity. a) Inhomogeneity in the presence of vegetation at the surface causes a decrease in $r_{\theta q}$ in rising air. b) Large humidity entrainment flux causes specific humidity to be not well-mixed, resulting in decorrelation of θ and q in sinking air (Note that a) only comprises -part of- the surface layer, whereas b) depicts the entire mixed layer)

purely based on observations, and corresponds to the results of Katul and Hsieh (1999) for Bowen ratios above 1. Lamaud and Irvine (2006) also provide an interpolation between the wet regime (low Bowen ratio) and dry regime (high Bowen ratio). This interpolation suggests that for a Bowen ratio of around 0.3 the dimensionless standard deviations of temperature and humidity will be equal, irrespective of the magnitude of $r_{\theta q}$.

We can conclude that although $|r_{\theta q}| < 1$ is a clear indication of a violation of one or more of the conditions for MOST, it is not possible to separate the influence of surface heterogeneity and entrainment.

2.4 *How to identify the influence of entrainment and surface heterogeneity*

2.4.1 Scalar skewness

Under unstable conditions the skewness of temperature is positive, reflecting the fact that updrafts with large positive temperature perturbations occur only during a small fraction of the time, whereas slow downdrafts are dominating. Tillman (1972) shows an upper limit of 1 for strongly convective conditions and a proportionality of the skewness to $\ln\left(\frac{z}{L}\right)$. This upper limit is confirmed by Andreas et al. (1998), whereas Ohtaki (1985) shows a limiting values of 0.5. He also shows that the skewnesses of humidity and CO_2 have the same absolute values as that of temperature, where the humidity skewness is positive and the carbon dioxide skewness is negative.

Mahrt (1991) analysed variances obtained from low-level aircraft observations. He shows that for drier surfaces the humidity skewness can deviate considerably from 1, decreasing with increasing dryness and even becoming negative. This negative skewness is associated with occasional patches of dry air originating from higher levels in the boundary layer (not necessarily from *above* the boundary layer, see figure 3a).

2.4.2 Time scale of scalar fluctuations

As long as processes in the surface layer dominate the scalar fluctuations, the time scale of those fluctuations will be limited to the time scale of the surface layer turbulence. The spectral peak for the temperature spectrum under unstable conditions is roughly located at $\frac{fz}{\bar{u}} \approx 0.02 - 0.05$, where f is the frequency and u is the mean wind speed (Kaimal et al., 1972). With a mean wind speed of 5 ms^{-1} and an observation height of 10 m this yields characteristic time scale of the order of 40-100 seconds.

On the other hand, if fluctuations in the surface layer are originating from higher levels in the boundary layer, or even from the entrainment layer, they may have a time scale of the order of the convective time scale $\frac{z_i}{w_*}$ where x_i is the boundary layer height and w_* is the convective velocity scale $(\frac{g}{\bar{\theta}}\overline{w'T'}z_i)^{1/3}$. With a surface heat flux of 200 W m^{-2} and a boundary layer height of 2000 m this would give a time scale of 900 seconds, i.e. an order of magnitude larger than the surface layer time scale.

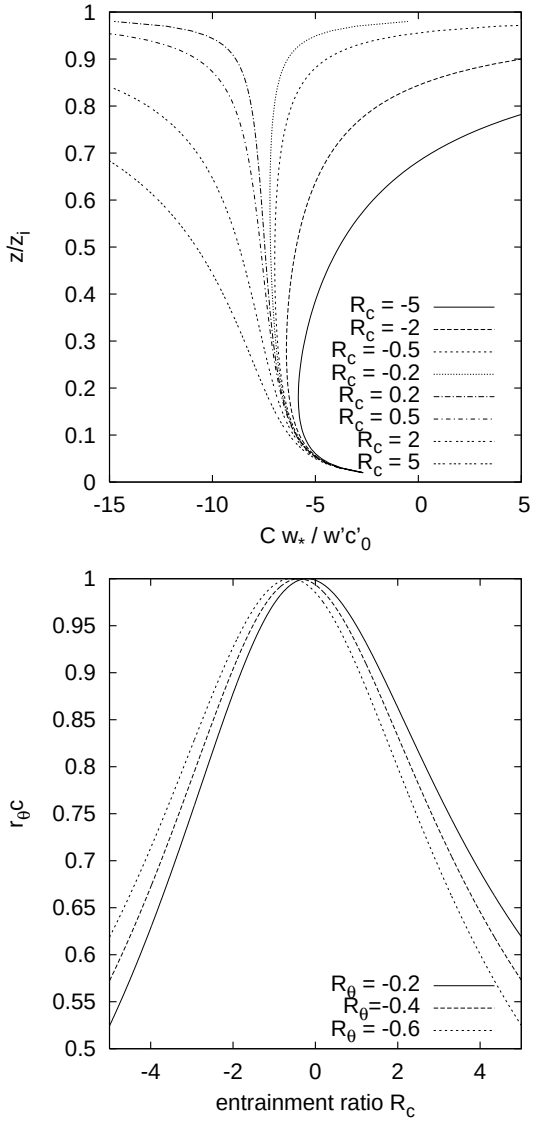

FIG. 3: Influence of entrainment on scalar correlation as derived from Moeng and Wyngaard (1989) a): dimensionless mean scalar concentration profiles for a range of scalar entrainment ratios, derived from the expressions in figure 11 in Moeng and Wyngaard (1989). b): Relationship between the entrainment ratio for a scalar, R_c and the correlation coefficient for θ and the scalar concentration c within the surface layer, i.e. z/z_i = 0.01.

3. Data

The analysis presented in this paper is mainly based on data from eddy-covariance stations. Those are discussed, together with characteristics of the two sites, in section 3.1. Some additional data is discussed in section 3.2.

3.1 *Eddy-covariance data*

The characteristics of the two sites, as well as the equipment employed, is given in table 1.

Although the instrumentation of the two experiments differed slightly, the processing of the eddy-covariance data was identical for both sites. From the raw data half-hourly fluxes have been computed taking into account the following corrections:

- the raw data have been linearly detrended;
- the mean signal of the Krypton hygrometer (CASES-99) has been adjusted using the humidity measurements of a slow-response sensor;
- axis rotation using the planar fit method, with planar fit angles determined on a 5-daily basis (see Wilczak et al. (2001)). The bias in the vertical velocity was was set to zero;
- sonic temperatures were corrected for humidity (see Schotanus et al. (1983));
- the oxygen-sensitivity of the Krypton hygrometer was corrected for using the coefficients found by van Dijk et al. (2003).
- corrections for frequency response and path averaging according to Moore (1986);
- the Webb-term for the water vapour flux (and CO_2 for Ghana) is taken into account (see Webb et al. (1980)).

For all computed quantities, the statistical error (tolerance) has been estimated using the method described in van Dijk et al. (2004). Assuming a normal distribution of the statistical errors, the real value of a quantity should be within the range of the computed value plus or minus the tolerance. This information on the statistical error will be used in the selection of reliable data, as well as in the fitting of similarity relationships. More details and software can be found in van Dijk et al. (2004) and at http://www.met.wau.nl/projects/jep.

Both data sets suffer from some data loss, albeit for different reasons. In the case of the Ghana dataset, power failures caused data loss, mostly during the night, in the last 2 weeks of the experiment. The CASES-99 dataset misses some daytime data, because all maintenance was done during the day since the experiment was focused on the stable boundary layer. Furthermore, instrumental problems caused missing samples. One cause was that during the first week the data logger program had to finish too many instructions. After removal of one thermocouple, this problem disappeared. Furthermore, the sonic anemometer exhibited some intermittent problems that later were solved by recalibration.

3.2 *Additional data*

In order to check the possible influence of entrainment processes, additional data regarding the boundary layer characteristics are needed. Since no radio soundings were available for the Ghanean data set, we have used profiles from the operational ECMWF model runs. The data (temperature, humidity and pressure) were downloaded from the MARS archive at the native model levels and interpolated vertically to a dense vertical grid.

4. Results

4.1 *Changes in fluxes during the observation period*

Figure 4 shows the change of the midday Bowen ratio for both sites. For Ghana the increase is from around 0.5 to around 3, whereas the CASES data already start out drier with a Bowen ratio equal to 1 and end at a value of around 4. Due to the fact that data loss in the CASES data was mainly occurring during daytime, the CASES data are a bit more scarce.

4.2 *Changes in the correlation coefficients*

The deviations from MOST which are the subject of this paper are caused by differences in source areas for the different scalars. As pointed out in section 2.2 those differences will lead to a decorrelation of the scalars. Figure 5 shows that r_{Tq} during daytime decreases from 0.9 to 0.25 between the start and the end of the season. For $r_{qq_{CO2}}$ a similar tendency can be found (except for the sign of the correlation coefficient). For stable conditions there is no clear trend through the season in terms of a decrease of the magnitude of the correlation coefficient. But what *can* be seen is that in the drier part of the season stronger stability occurs at night (a shift from $z/L \approx 0.01 - 0.1$ to $z/L \approx 1$.

4.3 *Changes in similarity functions*

Since the similarity relationships are defined in terms of the dimensionless group $(z - d)/L$, first the displacement height d needs to be determined. Especially for the Ghana data, gathered over savannah with scattered trees, this might be relevant. However, using the method of de Bruin and Verhoef (1997) it appears that the displacement height is negligible.

In order to reduce any unneeded scatter in the similarity relationships, a rather strict selection has been applied to the data:

- only data with a wind direction that is within $\pm 120^\circ$ of the orientation of the sonic anemometer is allowed;
- the tolerance in the wind direction should be less that $\pm 90^\circ$ (in order to make the former restriction meaningful);

Table 1: Main characteristics of the two datasets used.

	Ghana	CASES-99
coordinates	9°29' N, 0°55' W	37°39' N, 96°43' W
time (date)	November 4, 2002 - December 10, 2002	September 30, 1999 - October 28, 1999
time (DOY)	308-340	273-301
vegetation	savannah with bushes and trees	grassland
installation height	10 meter	3 meter
sonic anemometer	CSAT-3D (Campbell Scientific)	idem
hygrometer	IrGA 7500 (LiCor)	Krypton hygrometer (Campbell Scientific)
CO_2 sensor	IrGA 7500 (LiCor)	-

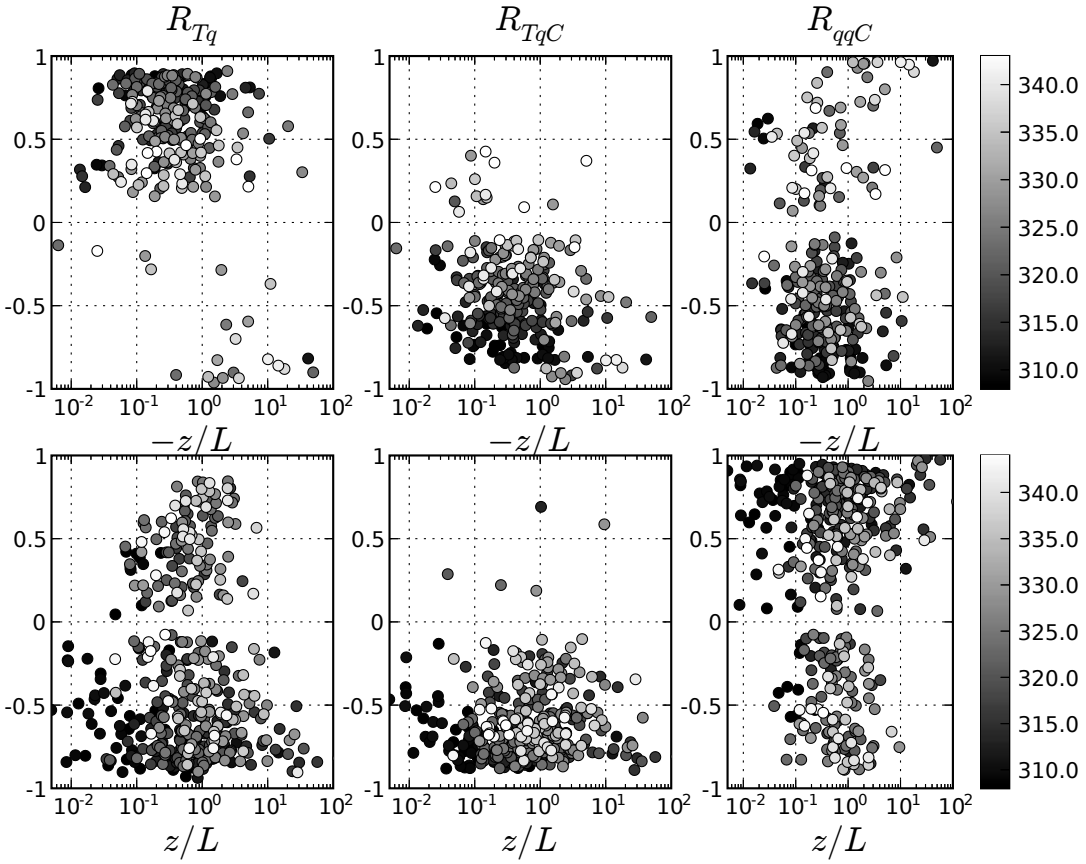

FIG. 5: Correlation coefficient between temperature and humidity (left), temperature and CO_2 (centre) and humidity and CO_2 (right) for unstable (top) and stable (bottom) conditions. Gray scale of dots indicates the daynumber of the observation. Data have been filtered to have a maximum error in both r_{xy} and z/L of 50%. Data are from the Ghana data set

.

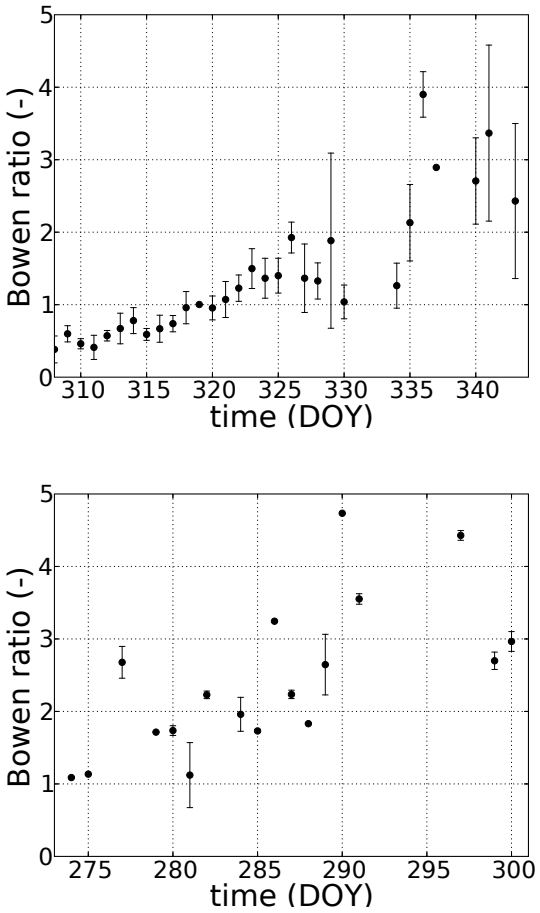

FIG. 4: Long term development of the Bowen ratio for the Ghana data (left) and CASES-99 data (right). Based on half-hourly fluxes, points indicate mean of Bowen ratios between 10 and 14 GMT (Ghana) or CDT (CASES), and the error bars indicate the standard deviation.

- the relative tolerance in the dimensionless groups occurring in the similarity relationships should be less that 20%. This tolerances is determined, based on the tolerances of the different quantities comprising a dimensionless group;

Figures 6 and 7 show the similarity relationships for both sites, for temperature, humidity and CO_2 (only Ghana). For both datasets, the similarity for σ_T shows least scatter, whereas the CO_2 data from Ghana shows most scatter. However, all unstable data exhibit the predicted $-\frac{1}{3}$ power dependence on *z/L*. Furthermore, the scatter for the stable side is more or less the same for all scalars.

In order to be able to compare the relationships for the different scalars and to quantify the scatter, the expressions of 5 and 6 were fitted to the data. The fitting was done using orthogonal distance regression. This method takes into account the tolerances of *both* two variables that are fitted by weighting the contribution of a given observation with a weight that is inversely proportional to the square of its error. Because the data do not cover near-neutral data, the transition between neutral and free-convection (i.e. $\frac{z}{L} \approx C_{xu2}^{-1}$ could not be determined accurately). Therefore, C_{xu2} was fixed to a value of 28.4 (de Bruin et al., 1993).

To investigate a possible relationship between the scatter in the relationships for q and q_C and the change in surface fluxes, the data was split into two periods: a relatively wet and a dry period (period 1 and period 2). The results can be found in table 2 and are also given as regression lines in figures 6 and 7. From the numbers in the table, a number of conclusions can be drawn:

- The values for C_{Tu1} are close for both experiments and both periods, but for the CASES dataset the first period differs significantly from the other period.
- For the Ghana data, C_{qu1} changes significantly between the two periods, from a value close to C_{Tu1} to a value 23% higher.
- The value of C_{Cu1} for Ghana is much higher than C_{Tu1} for both periods.
- For the stable part of the Ghana data, C_{qs} and C_{Cs} are close, and higher than C_{Ts}. In the second period the difference between C_{Ts} on the one hand, and C_{qs} and C_{Cs} on the other is larger.
- In the CASES data C_{qu1} increases from period 1 to period 2, but this change is not statistically significant.
- For all data, the coefficients for water vapour and CO_2 are higher than those for temperature.

The parameterization of Lamaud and Irvine (2006) (as well as the analysis of Katul and Hsieh (1999)) suggest that for $\beta > 1$ the ratio of $\frac{C_{qu1}}{C_{Tu1}} = r_{Tq}^{-1}$. However, in our data $\frac{C_{qu1}}{C_{Tu1}} = 1.23$ whereas r_{Tq}^{-1} is of the order of 2-4

(see figure 5). Thus estimation of $\frac{C_{qu1}}{C_T u1}$ from r_{Tq}^{-1} would overestimate the effect of decorrelation on the similarity relationships.

4.4 *Indications for causes for non-MOST behaviour*

Since the largest non-MOST behaviour in the similarity relationships has been observed for the Ghana dataset, this section will focus on those data only.

4.4.1 Scalar skewness

Figure 8 shows the variation through the day and through the season of the skewnesses of vertical wind speed and the scalars under consideration for the Ghana data set. It appears that the skewness for the vertical wind speed is well-defined and varies in a limited range. The temperature skewness has a larger diurnal cycle, but does not change through the season. On the other hand, the skewness for humidity and CO_2 do change through the season. For both scalars, the absolute value decreases with day number (and so with drying conditions). This indicates that the humidity and CO_2 fluctuations become more and more normally distributed and do not show that large skewness of temperature that is indicative of the convective motions. The low values for the skewnesses of q and q_c could be interpreted as an increased importance of entrainment processes (Mahrt, 1991).

4.4.2 Time scale of scalar fluctuations

Figure 9 shows that the character of the scalar fluctuations differs considerably between a day in the wet period and a day in the dry period (days 308 and 340, respectively). Whereas the fluctuations of vertical wind speed and temperature look similar, the fluctuations of q and q_c go from fluctuations with a short time scale (comparable to that of T) to fluctuations with a long time scale.

This observation can also be quantified by looking at the integral time scales of the fluctuations. Here we have computed that integral timescale from the ogives (Oncley et al., 1996) of the different quantities. We defined the integral scale is as that timescale where 50% of of the variance has been covered by the ogive. The resulting time scales are shown in figure 10. During daytime the vertical wind speed fluctuations have a typical time scale of the order of one minute. The temperature signal has a somewhat larger time scale of about 100 seconds. At the start of the observation period, humidity and CO_2 have timescales very similar to those of temperature. However, when the drying of the surface progresses, the time scales of humidity and CO_2 increase to values close to 1000 seconds. Especially for humidity the trend is clear. The increase of the timescale can be interpreted as an increasing importance of large scale fluctuations orginating from the upper part of the boundary-layer or perhaps from in or above the entrainment zone. This tendency fits very well with the examples shown in figure 9.

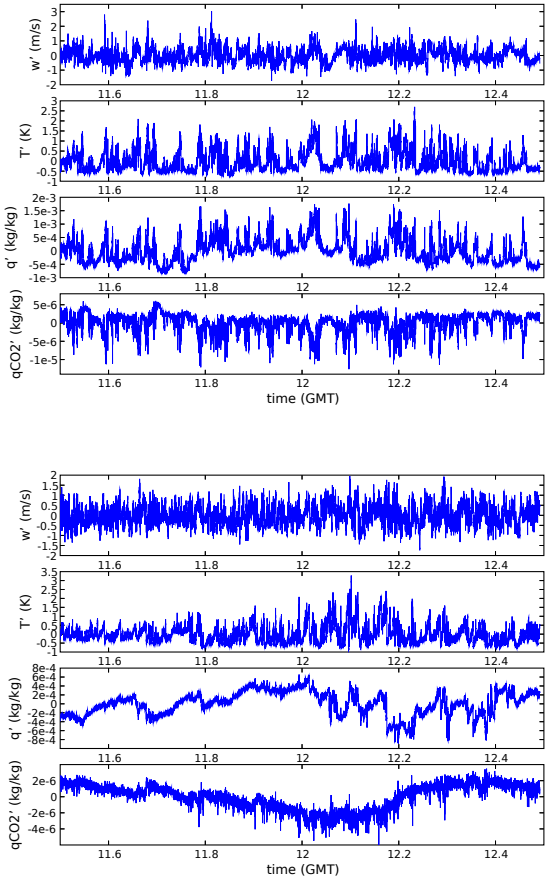

FIG. 9: Ghana data: fluctuations of vertical wind speed, temperature, specific humidity and specific CO_2 on days 308 (top) and 340 (bottom).

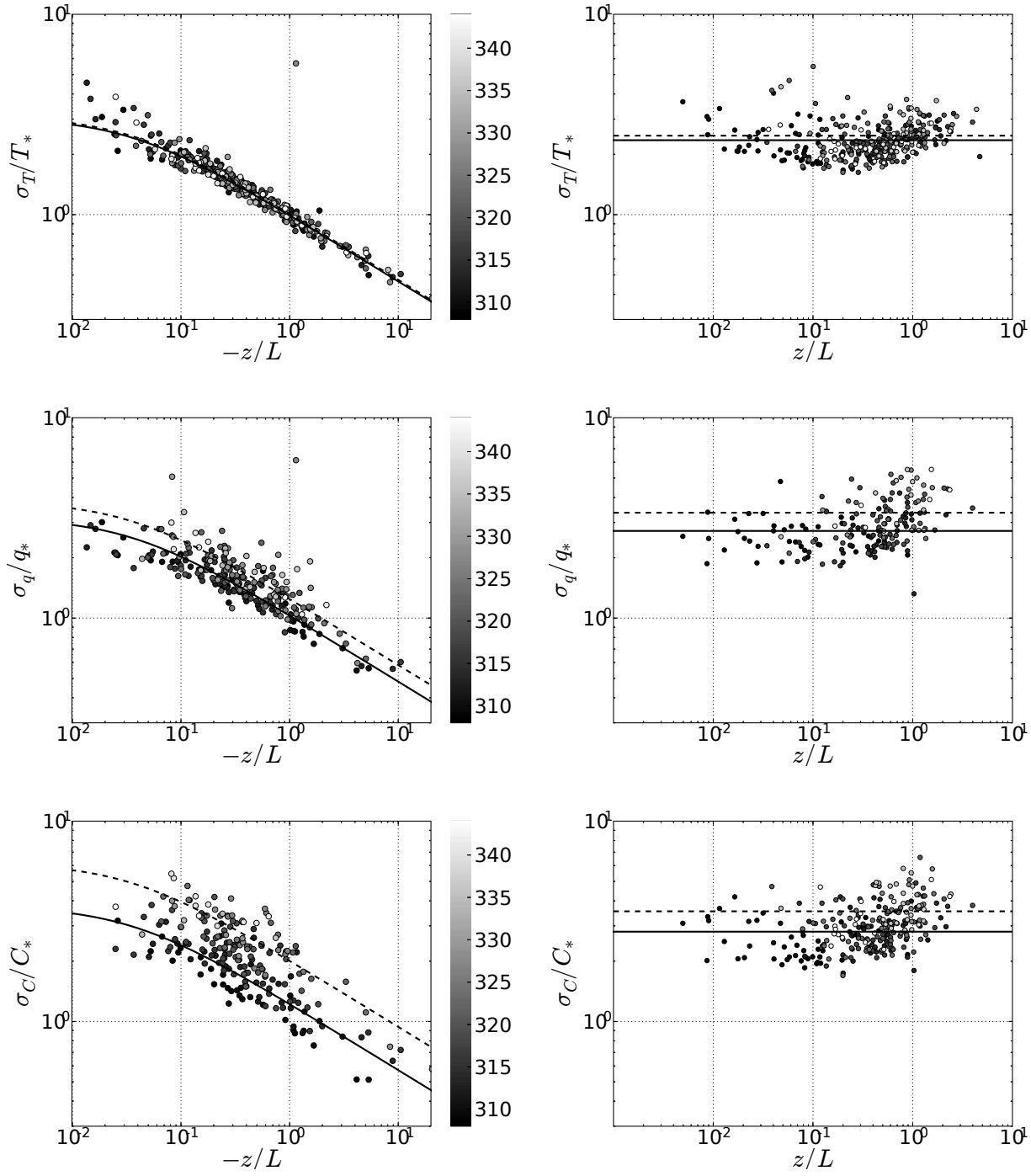

FIG. 6: Ghana data: similarity relationship for scalar standard deviation for unstable (left) and stable (right) situations, for temperature (top), specific humidity (middle) and CO_2 (bottom). The gray scale bar indicates that DOY of the observation. The lines are fits to the data for the period until DOY 325 (full line) and after DOY 325 (dashed line).

Table 2: Coefficients in the similarity relationships for the scalar standard deviations (equation 5). The coefficient C_{xu2} has been kept constant at a value of 28.4, since near-neutral data were scarce. For Ghana periods 1 and 2 refer to DOY 308-325 and 326-340. For CASES this is: DOY 273-285 and 286-301. Also given is the free-convection coefficient A_{xu}, used in equation 2.

		Period 1			Period 2		
dataset	coefficient	value	tolerance	N	value	tolerance	N
Ghana	C_{Tu1}	3.05 (A_{Tu} = 1.00)	0.04	149	3.11 (A_{Tu} = 1.02)	0.08	205
	C_{qu1}	3.17 (A_{qu} = 1.04)	0.07	135	3.83 (A_{qu} = 1.26)	0.14	121
	C_{Cu1}	3.76 (A_{Cu} = 1.23)	0.15	131	6.19 (A_{Cu} = 2.03)	0.30	81
	C_{Ts}	2.35	0.06	179	2.48	0.09	161
	C_{qs}	2.72	0.12	120	3.36	0.21	60
	C_{Cs}	2.81	0.11	142	3.55	0.18	117
CASES	C_{Tu1}	3.19 (A_{Tu} = 1.05)	0.09	72	3.01 (A_{Tu} = 0.99)	0.05	87
	C_{qu1}	3.46 (A_{qu} = 1.13)	0.12	69	3.56 (A_{qu} = 1.17)	0.10	84
	C_{Ts}	2.56	0.09	156	2.80	0.10	225
	C_{qs}	3.12	0.11	98	3.34	0.16	111

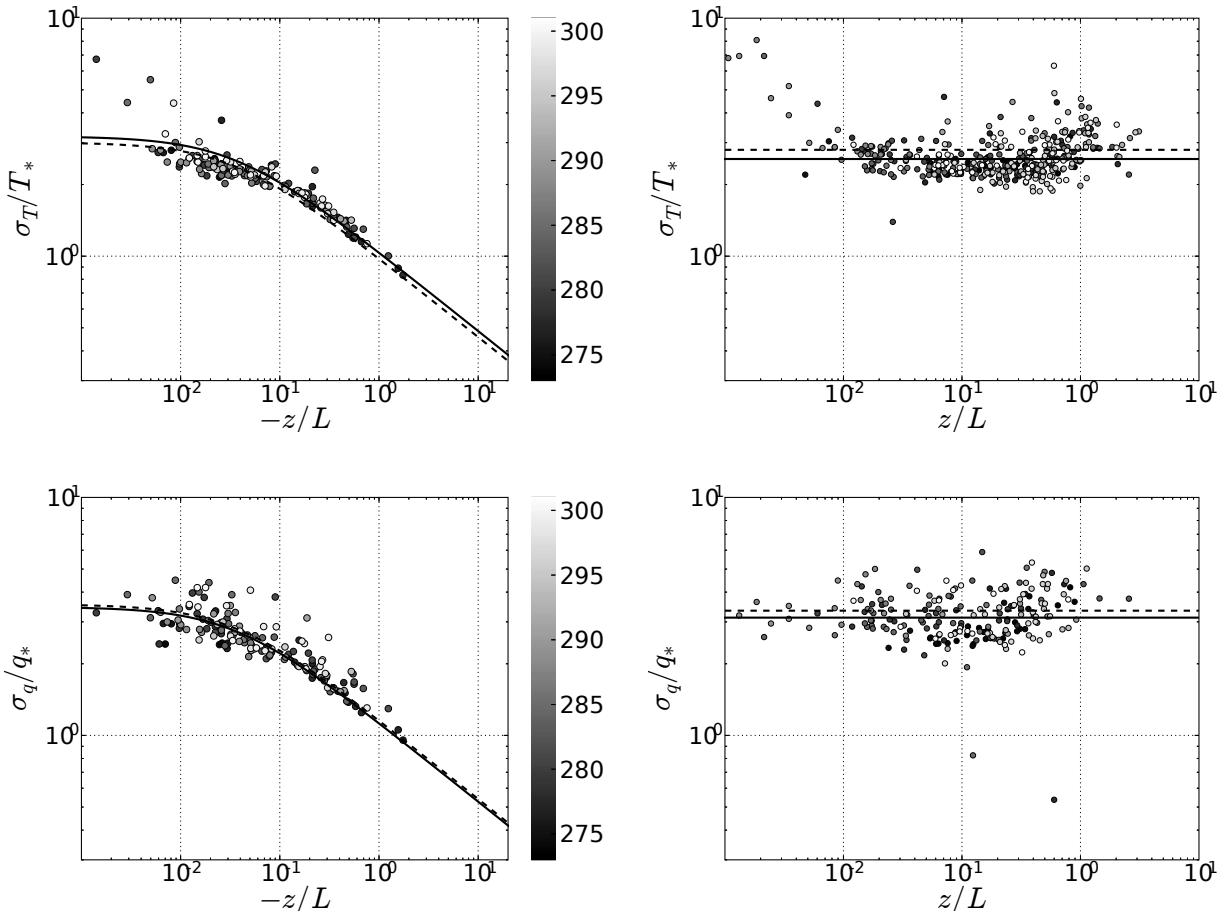

FIG. 7: CASES data: similarity relationship for scalar standard deviation for unstable (left) and stable (right) situations, for temperature (top), specific humidity (middle) and CO_2 (bottom). The gray scale bar indicates that DOY of the observation. The lines are fits to the data for the period until DOY 285 (full line) and after DOY 285 (dashed line).

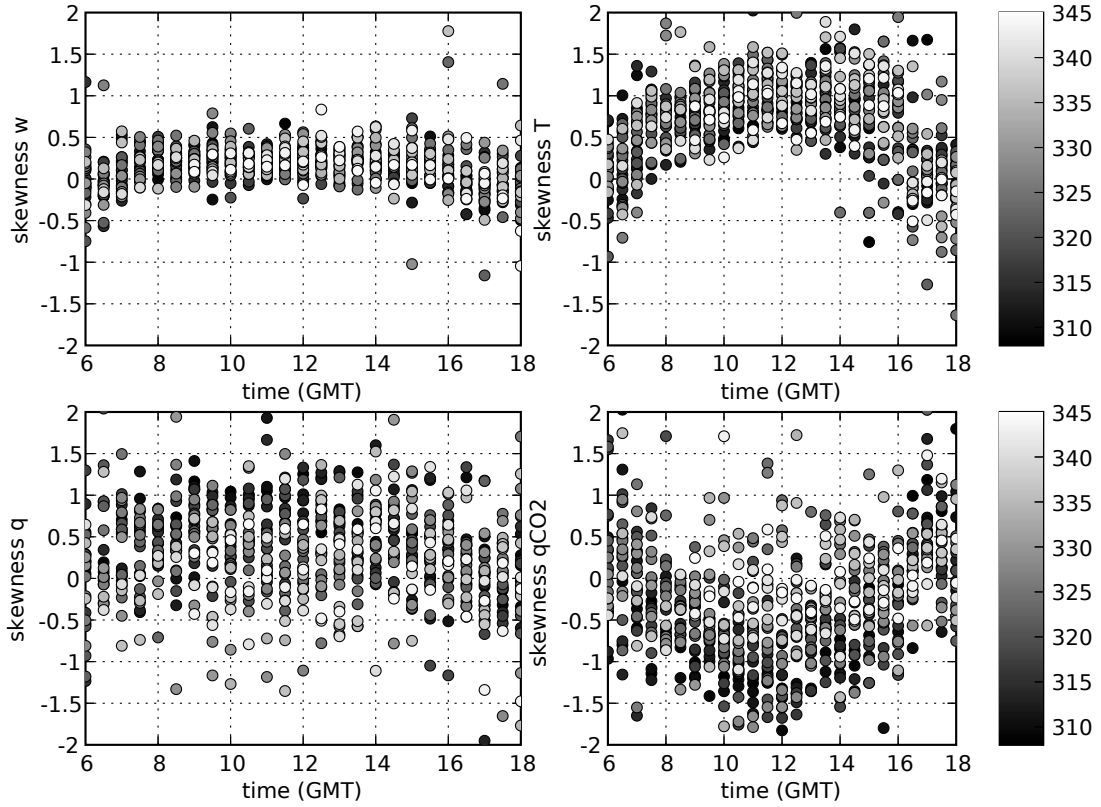

FIG. 8: Variation of the skewness of vertical wind speed (upper left), temperature (upper right), specific humidity (lower left) and specific CO_2 concentration (lower right) during the day and through the season (indicated by the colours, signifying the day number). Data are from the Ghana data set.

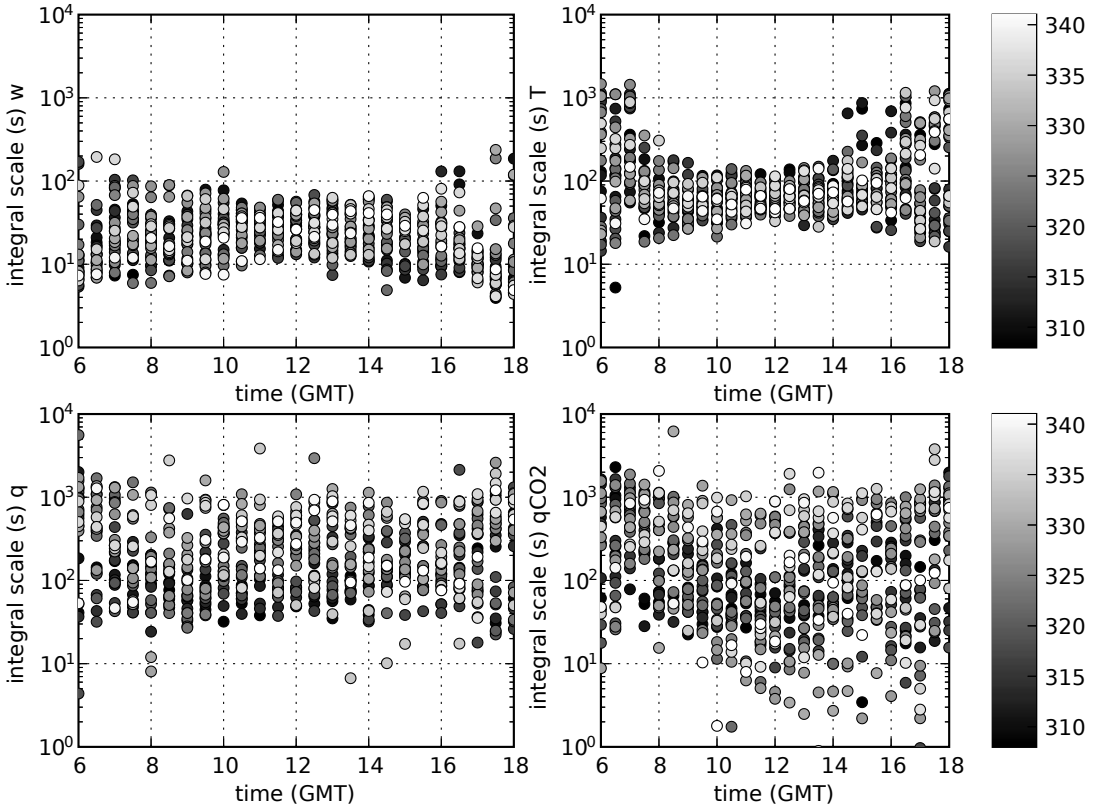

FIG. 10: Variation of the integral timescale of vertical wind speed (upper left), temperature (upper right), specific humidity (lower left) and specific CO_2 concentration (lower right) during the day and through the season (indicated by the gray scales, signifying the day number). Data are from the Ghana data set

.

4.4.3 ENTRAINMENT RATIO FOR HUMIDITY

In the previous sections it was shown that it is likely that entrainment processes are at least in part responsible for the decorrelation of T and q fluctuations. We have derived the entrainment Bowen ratio (β_{entr}, ratio of entrainment heat flux to entrainment latent heat flux) as $\frac{\Delta\theta}{\Delta q}$ where $\Delta\theta$ and Δq are the temperature and humidity jump at the top of the boundary layer. Those were determined from the ECMWF-model profiles by combining the model profiles with a mixed-layer template: extrapolate the constant mixed layer concentration upward, extrapolate the free-atmosphere concentration gradient downward, and determine the jump from the distance between both lines at $z = z_i$ (z_i determined by lifting an air parcel with an excess temperature of 1 K from 20 meters). For the Ghana data this yielded for the 12 GMT field an entrainment Bowen ratio between -0.15 and -0.25 throughout the entire experiment, without a clear trend in time.

The entrainment ratio for humidity R_q can be determine from β_{entr}, the surface Bowen ratio β and the entrainment ratio for heat R_θ in the following way:

$$R_q = R_\theta \frac{\beta}{\beta_{entr}} \tag{7}$$

Given the fact that the entrainment ratio for heat has a limited range and it was observed above that the entrainment Bowen ratio is also constant in time, 7 implies that the entrainment ratio for water vapour varies according to the surface Bowen ratio. With $R_\theta \approx -0.2$ and $\beta_{entr} = -0.2$, R_q varies from 0.5 to 3 (with β according to figure 4). This indeed indicates a transition from a surface flux dominated regime to an entrainment flux dominated regime.

For the CASES-99 data (where we used the 18 GMT fields) the β_{entr} is more variable between days with values ranging roughly from -0.5 to -1.5. These larger values imply that the the entrainment ratio for moisture is smaller and of the order of 0.2 to 0.6 (using $R_\theta = -0.2$, $\beta_{entr} = -1$ and the range of β shown in figure 4). These lower entrainment ratio for moisture may explain the fact that in the CASES-99 data no MOST-deviations are found, even though the drying up is comparable to that in the Ghana data.

5. Conclusion

The influence of non-ideal conditions on the similarity relationships for scalar variances has been investigated using data from two different sites. Both datasets have in common that the surface Bowen ratio increases strongly in one month time. The data differ with respect to the homogeneity of the surface: the CASES-99 data refer to a homogeneous case, whereas the Ghana data have a surface heterogeneity that increases in time as the grass between the trees dies.

Only the data from Ghana show deviations from MOST for q (and q_{CO2}) in the dry period, whereas the CASES-99 data show MOST-behaviour both in the moist part of the data set and in the dry part, both for θ and for q. Based on the development of the time scale of the scalar fluctuations, as well as on the development of the scalar skewness there are strong indications that entrainment influences the scalar turbulence in the surface layer. This is consistent with the increasing entrainment ratio for humidity that is derived from ECMWF-model fields. However, deviations from MOST at night suggest that the surface heterogeneity causes non-MOST behaviour as well.

REFERENCES

Andreas, E. L., R. J. Hill, J. R. Gosz, D. I. Moore, W. D. Otto, and A. D. Sarma, 1998: Statistics of surface-layer turbulence over terrain with metre-scale heterogeneity. *Boundary-Layer Meteorology*, **86**, 379–408.

Beljaars, A.C.M., P. Schotanus, and F.T.M. Nieuwstadt, 1983: Surface layer similarity under nonuniform fetch conditions. *J. Clim. Appl. Meteorol.*, **22**, 1800–1810.

de Arellano, J. V.-G, B. Gioli, F. Miglietta, H. J. J. Jonker, H. Klein Baltink, R. W. A. Hutjes, and A. A. M. Holtslag, 2004: Entrainment process of carbon dioxide in the atmospheric boundary layer. *J. Geophys. Res.*, **109**, D18110.

de Bruin, H.A.R. and A. Verhoef, 1997: A new method to determine the zero-plane displacement. *Boundary-Layer Meteorology*, **82**, 159–164.

de Bruin, H. A. R., N. J. Bink, and L. J. M. Kroon, 1991: Fluxes in the surface layer under advective conditions. In *Land Surface Evaporation*, Schmugge, T. J. and André, J. C., editors. 157-171.

de Bruin, H. A. R., W. Kohsiek, and B. J. J. M. van den Hurk, 1993: A verification of some methods to determine the fluxes of momentum, sensible heat, and water vapour using standard deviation and structure parameter of scalar meteorological quantities. *Boundary-Layer Meteorology*, **63**, 231–257.

Druilhet, A., J. P. Frangi, D. Guedalia, and J. Fontan, 1983: Experimental studies of the turbulence structure parameters of the convective boundary layer. *J. Clim. Appl. Meteorol.*, **22**, 594–608.

Hartogensis, O.K., H.A.R. DeBruin, and B.J.H. van de Wiel, 2002: Displaced-beam small aperture scintillometer test. Part II: CASES-99 stable boundary layer experiment. *Boundary-Layer Meteorology*, **105**, 149–176.

Hill, R. J., 1989: Implications of Monin-Obukhov similarity theory for scalar quantities. *J. Atmos. Sci.*, **46**, 2236–2251.

Kaimal, J. C., J. C. Wyngaard, Y. Izumi, and O. R. Coté, 1972: Spectra characteristics of surface-layer turbulence. *Q. J. R. Meteorol. Soc.*, **98**, 563–589.

Katul, G., S.M. Goltz, C-I. Hsieh, Y. Cheng, F. Mowry, and J. Sigmon, 1995: Estimation of surface heat and momentum fluxes usnig the flux-variance method above uniform and non-uniform terrain. *Boundary-Layer Meteorology*, **74**, 237–260.

Katul, G.G. and C-I. Hsieh, 1999: A note on the flux-variance similarity relationships for heat and water vapour in the unstable atmospheric surface layer. *Boundary-Layer Meteorology*, **90**, 327–338.

Lamaud, E. and M. Irvine, 2006: Temperature-humidity dissimilarity and heat-to-water vapour transport efficiency above and within a pine forest canopy: the role of the bowen ratio. *Boundary-Layer Meteorology* DOI 10.1007/s10546–005–9032–6.

Mahrt, L., 1991: Boundary-layer moisture regimes. *Q. J. R. Meteorol. Soc.*, **117**, 151–176.

Michels, B. I. and A. M. Jochum, 1995: Heat and moisture flux profiles in a region with inhomogeneous surface evaporation. *J. of Hydrol.*, **166**, 383–407.

Moeng, C. H. and J. C. Wyngaard, 1989: Evaluation of turbulent transport and dissipation closures in second-order modeling. *J. Atmos. Sci.*, **46**, 2311–2330.

Moore, C. J., 1986: Frequency response corrections for eddy correlation systems. *Boundary-Layer Meteorology*, **37**, 17–35.

Ohtaki, E., 1985: On the similarity in atmospheric fluctuations of carbion dioxide, water vapor and temperature over vegetated fields. *Boundary-Layer Meteorology*, **32**, 25–37.

Oncley, S. P., C. A. Friehe, J. C. Larue, J. A. Businger, E. C. Itsweire, and S. S. Chang, 1996: Surface-layer fluxes, profiles, and turbulence measurements over uniform terrain under near-neutral conditions. *J. Atmos. Sci.*, **53**, 10291044.

Roth, M. and T.R. Oke, 1995: Relative Efficiencies of turbulent transfer of heat, mass, and momentum over a patchy urban surface. *J. Atmos. Sci.*, **52**, 1863–1874.

Schotanus, P., F. Nieuwstadt, and H. DeBruin, 1983: Temperature measurement with a sonic anemometer and its application to heat and moisture fluxes. *Boundary-Layer Meteorology*, **26**, 81–93.

Schüttemeyer, D., A.F. Moene, A.A.M. Holtslag, H.A.R. de Bruin, and N van de Giesen, 2006: Surface fluxes and characteristics of drying semi-arid terrain in West Africa. *Boundary Layer Meteorology* DOI 10.1007/s10546–005–9028–2.

Sorbjan, Z., 1991: Evaluation of local similarity functions in the convective boundary layer. *J. Appl. Meteor.*, **30**, 1565–1583.

Tillman, J.E., 1972: The indirect determination of stability, heat and momentum fluxes in the atmospheric boundary layer from simple scalar variables during dry unstable conditions. *J. Appl. Meteor.*, **11**, 783–792.

van Dijk, A., W Kohsiek, and H.A.R. de Bruin, 2003: Oxygen sensitivity of krypton and Lyman-alpha hygrometers. *J. Atmos. Ocean. Tech.*, **20**, 143–151.

van Dijk, A., A.F. Moene, and H.A.R de Bruin, 2004: The principles of surface flux physics: theory, practice and description of the {ECPACK} library. Internal report 2004/1, Wageningen University, Meteorology and Air Quality Group.

Webb, E., G. Pearman, and R. Leuning, 1980: Correction of flux measurements for density effects due to heat and water vapour transfer. *Q. J. R. Meteorol. Soc.*, **106**, 85–100.

Wilczak, J.M., S.P. Oncley, and S.A. Stage, 2001: Sonic anemometer tilt correction algorithms. *Boundary-Layer Meteorology*, **99**, 127–150.